Spectral properties of one-dimensional $(AB)^N(BA)^N$ photonic crystal containing double-negative and single-negative metamaterials

ZHOU GE[a], DAN ZHAO[b], JIAN-WEI WU[a,*]
[a]*School of Physics and Electronic Engineering, Chongqing Normal University, Chongqing 401331, People's Republic of China*
[b]*State Key Laboratory on Integrated Optoelectronics, Jilin University, Changchun 130012, People's Republic of China*

We present and study theoretically the photonic properties of transmission spectra in one-dimensional binary photonic crystal with $(AB)^N(BA)^N$ structure composed of alternate double-negative and single-negative metamaterials. The Bragg band gap, defect mode, special band gap and special resonance mode of output spectrum are directly related to the layer thickness, lattice constant, period number, incident angle, as well as material parameters including electric permittivity and magnetic permeability. In the cases of oblique incidence and TE polarization wave, a special resonance mode is generated in the special band gap. By changing the incident angle, ranging from 0^0 to 85^0, the defect mode in the Bragg band gap is moved to higher frequency, and the resonance mode in the special band gap is red-shifted and further splits into multiple peaks.

(Received December 4, 2017; accepted October 10, 2018)

Keywords: Photonic crystals, Metamaterials, Defect mode and band gaps

1. Introduction

Photonic crystal (PC) is the prominently artificial structure that is periodically arranged by the various dielectric layers [1]. According to the stacking form, the PC is classified into three types including one-dimensional [2], two-dimensional [3] and three-dimensional organizations [4], in which the one-dimensional PC (1D PC) has been intensively proposed and investigated because of simple design and operation [5-8]. Conventionally, the materials with different positive refractive indexes are, respectively, selected as the stacking layers of 1D PC, in which the reflection waves arising from the interface between two layers will induce the strong interference effect under Bragg scattering condition, resulting in the generation of Bragg band gap. Additionally, the defect mode in the Bragg band gap is also achieved by introducing the defect layer that destroys the periodical array of multilayers structure. Therefore, based on the optical properties of Bragg band gap and defect mode, the PC has been extensively used to perform numerous optical technologies such as filter [9], dispersion compensation [10], laser [11], slow light [12], phase retarder [13], optical switching [14], biosensors [15], omnidirectional reflector [16], resonator [17], harmonic generation [18], as well as optical beam splitter [19]. Even so, the 1 D PC based technology is seriously limited due to the very sensitive behavior of widths and central positions of Bragg band gap and defect mode to the layer thickness, lattice constant, and incident angle [20]. As a consequence, some metamaterials such as double-negative material (DNG) and single-negative material (SNG) that are employed in PC are proposed and theoretically studied in detail over the past decade. These types of metamaterials have obvious distinctions on the basis of the signs of two material parameters including electric permittivity (ε-epsilon) and magnetic permeability (μ-mu) [21-24], i.e., double-negative material with simultaneously negative epsilon and negative mu, epsilon-negative material (ENG) with negative epsilon, but positive mu, and mu-negative material (MNG) with negative permeability, but positive permittivity. So, the SNG material has two types including ENG and MNG material. In comparison to the conventional material with positive refractive index, the metamaterials have some unique optical features such as negative refractive index, imaginary refractive index, evanescent electromagnetic, reversal Snell's law, and reversed Doppler effect and reversed Cerenkov radiation [25, 26]. Although both DNG and SNG materials aren't found in nature now, they are artificially fabricated, and successfully utilized in photonic crystal. Hence, some novel photonic band gaps such as zero-average refractive index band gap, zero-effective phase band gap, zero-permittivity band gap, zero-permeability band gap

which are originated from the essential physical mechanisms of metamaterials are obtained in the 1D PC containing metamaterials [27-29], in which the changes of optical characteristics for generated photonic band gaps are fully different from the cases of conventional Bragg band gap caused by the multiple interferences while varying the layer thickness and incident angle. In reality, the photonic properties of metamaterials based 1D PC still need to be further explored and investigated for attaining some significant results that will promote the PC containing metamaterials to solve some challenging technologies that cannot be overcome by the conventional PC consisting of various dielectric layers with positive refractive indexes. In this work, we present the 1D PC in the form of $(AB)^N(BA)^N$ composites, in which both *A* and *B* layers denote the DNG material and ENG material, respectively. Although the 1D PC with alternately stacked DNG and ENG material films have already been presented in previous report [30], both a special band gap and defect mode in the Bragg band gap have been analyzed in the cases of normal incidences and various layer thicknesses. Using this design setup in this study, it is possible that more significant results can be found by selecting various material parameters, i.e., permittivity and permeability, incident angle, as well as structural parameters including layer thickness, and lattice constant. Consequently, one believes that these interesting optical properties in the presented 1D PC consisting of DNG and ENG material layers will have some potential applications in various technologies.

2. Model and theory

Fig. 1 displays the diagram schematic of 1D PC in the form of $(AB)^N(BA)^N$ that is composed of alternate double-negative material (labeled as layer *A*) and epsilon-negative material (labeled as layer *B*). The number of periodic cell unit (*AB* and *BA*) is *N*. The spatial period denoted by d_A+d_B is the thickness of a binary unit cell, and the proposed device is surrounded by air. The thicknesses of layer *A* and layer *B* are d_A and d_B, respectively. Let the incident plane wave with TE polarization state to be introduced into the PC, and propagate along the *Z* direction. The incident angle that is angle between incident wave and transmission direction is θ. Obviously, the joining part between $(AB)^N$ and $(BA)^N$, i.e., both of layers *B*, is as the defect layer of total multilayers structure whose geometrical length is extended to $2d_B$.

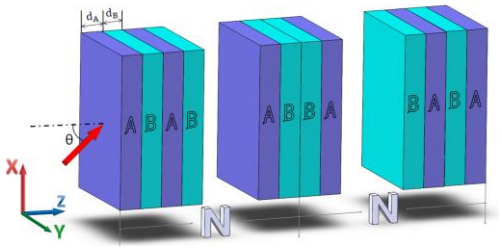

Fig. 1. Schematic diagram of 1D PC containing double-negative and epsilon-negative materials

Based on the Drude models and lossless condition, both electric permittivity ε_D and magnetic permeability μ_D parameters in the DNG material are, respectively, described as

$$\varepsilon_D = \varepsilon_{D0} - \frac{\omega_{ep}^2}{\omega^2} \tag{1}$$

$$\mu_D = \mu_{D0} - \frac{\omega_{mp}^2}{\omega^2} \tag{2}$$

and ε_E and μ_E in the ENG material are given by

$$\varepsilon_E = \varepsilon_{E0} - \frac{\omega_{ep}^2}{\omega^2} \tag{3}$$

$$\mu_E = \mu_{E0} \tag{4}$$

Here ω_{ep} and ω_{mp} with unit of GHz are the electronic plasma frequency and magnetic plasma frequency, respectively. ω with GHz unit is the angular frequency of incident wave. ε_{D0}, ε_{E0}, μ_{D0}, and μ_{E0} are the constants that can be fixed at various values to obtain different refractive indexes in numerical calculation.

In order to obtain the transmission spectra of incident wave in the presented PC, the transfer matrix method (TMM) that is an effective tool for analyzing the spectral properties such as photonic band gaps, and defect modes, is often used in simulation. Let an optical beam with TE polarization state be incident from air at an angle θ onto the structure. The electric field at two surfaces of any layer *A* or *B*, i.e., *z* and *z*+*d* positions, can be related via a characteristic matrix, expressed as [31]

$$M_h(d,\omega) = \begin{bmatrix} \cos(k_n^h d) & -\sin(k_n^h d)/q_n^h \\ q_n^h \sin(k_n^h d) & \cos(k_n^h d) \end{bmatrix} \tag{5}$$

Here *d* is the thickness of layer *A* or *B* that can be written as d_A or d_B, again, and superscript *h* denotes the h_{th} layer, as well as the subscript *n* indicates the *A* or *B* layer. For TE wave, the parameter *q* and the wave vector *k*, corresponding their *z* component in any layer, are written as

$$q_n^j = \sqrt{\varepsilon_n}/\sqrt{\mu_n}\sqrt{1-[\sin^2\theta/(\varepsilon_n\mu_n)]} \tag{6}$$

$$k_n^j = \omega/c\sqrt{\varepsilon_n}\sqrt{\mu_n}\sqrt{1-[\sin^2\theta/(\varepsilon_n\mu_n)]} \quad (7)$$

Here the constant c is the light velocity in vacuum. Accordingly, the characteristic matrix of each unit cell (AB or BA) in the j_{th} period can be given by

$$M_{AB} = \begin{bmatrix} \cos(k_A^j d_A) & -\sin(k_A^j d_A)/q_A^j \\ q_A^j \sin(k_A^j d_A) & \cos(k_A^j d_A) \end{bmatrix} \begin{bmatrix} \cos(k_B^j d_B) & -\sin(k_B^j d_B)/q_B^j \\ q_B^j \sin(k_B^j d_B) & \cos(k_B^j d_B) \end{bmatrix} \quad (8)$$

$$M_{BA} = \begin{bmatrix} \cos(k_B^j d_B) & -\sin(k_B^j d_B)/q_B^j \\ q_B^j \sin(k_B^j d_B) & \cos(k_B^j d_B) \end{bmatrix} \begin{bmatrix} \cos(k_A^j d_A) & -\sin(k_A^j d_A)/q_A^j \\ q_A^j \sin(k_A^j d_A) & \cos(k_A^j d_A) \end{bmatrix} \quad (9)$$

As a consequence, the total characteristics matrix M_T for the PC is written as

$$M_T = \begin{bmatrix} M_{11} & M_{12} \\ M_{21} & M_{22} \end{bmatrix} = \prod M_{AB}^1 M_{AB}^2 \ldots M_{AB}^N M_{BA}^1 M_{BA}^2 \ldots M_{BA}^N \quad (10)$$

Here M_{ab} (a, b=1,2) are the matrix elements of total transmission matrix M_T that will connect the incident end and the exit end. So, that the power transmittance $T(\omega)$ of incident plane wave through the PC can be given by

$$T(\omega) = \left| \frac{2\cos\theta}{(M_{11}+M_{22})\cos\theta + i(M_{12}\cos^2\theta - M_{21})} \right|^2 \quad (11)$$

Based on the given transmission matrix method, the transmission spectra of 1D PC can be analyzed and discussed by selecting various parameters such *as* polarization state, incident angle, period number, layer thickness, lattice constant, permittivity, as well as permeability.

3. Results and discussion

In the case of normal incidence, Fig. 2 displays the output spectrum of a plane wave with TE polarization state at the end of the presented 1D PC. In calculation, other material parameters including ε_{D0}=2, μ_{D0}=4, ε_{E0}=1, μ_{E0}=3. Both the special band gap and Bragg band gap are simultaneously exhibited in this illustration, in which the Bragg band gap is as a result of multiple interferences of multilayered reflections by the interface between two adjacent layers, and the special band gap is originated from the physical interaction of propagating waves and evanescent waves. In calculation, it is found that, under the absence of ENG material layer condition, a special band gap can be also achieved in enough thick DNG material layer, where the width of special band gap is remarkably narrower than that shown in Fig. 2. However, the corresponding results aren't shown in this plot. On the basis of the Drude model, both permittivity and permeability are related to the angular frequency, whose values will determine the signs of epsilon- and mu-parameters. So, after the frequency of incident wave is increased to enough high value, the refractive indexes, $n_{A,B}=(\varepsilon_{D,E})^{1/2}(\mu_{D,E})^{1/2}$, for layer A and B become positive. In this case, the optical properties of adopted materials are similar to those of conventional dielectrics with positive permittivity and permeability under the nonlinear interaction between incident wave and photonic crystals with the result that the conventional Bragg band gap is observed at the output port of 1D PC by selecting the incident wave with enough high frequency. Contrarily, as the angular frequency is decreased down to about 1 GHz in Fig. 2, both epsilon- and mu-parameters become zero or negative values. The direct result is that a special band gap is attained in the low frequency region, arising from the combined optical features of DNG and ENG materials. Additionally, The jointing location between $(AB)^N$ and $(BA)^N$, both of two layers B, are considered as a defect layer for the total PC structure so that a localized defect mode induced by the resonance frequencies of defect layer is occurred within the Bragg band gap. In simulation, one can find that the width of achieved photonic band gaps have no remarkable change by increasing the period number from 5 to 50, in which it is very surprising that the full width of half maximum (FWHM) of defect mode is quickly compressed from ~0.36 GHz to ~3.8 Hz, as shown in Fig. 3 (a). On the other hand, the output peak of defect mode plotted in Fig. 3(b) is always kept at a constant of 100% with the increase of period number. Here, it should be pointed out that the defect layer with enough long thickness that destroys the order periodic structure of total PC has no significant influence on the special band gap that is independent on the multilayers structure, and directly related to the thicknesses of metamaterials layers.

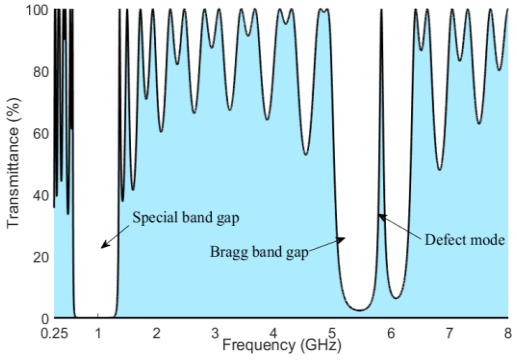

Fig. 2. Transmission spectrum with N=8, and 6 mm thickness for each layer A and B

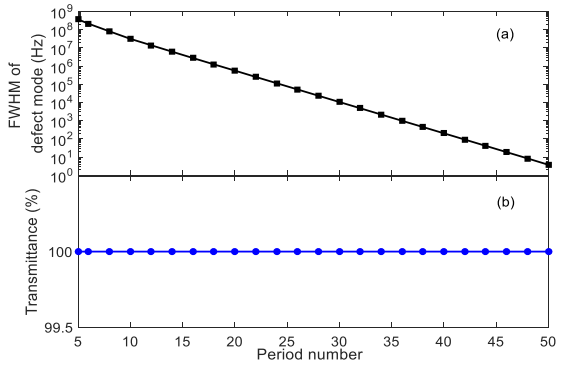

Fig. 3. With the increase of period number, (a). FWHM, and (b). Transmittance of the defect mode in Bragg band gap

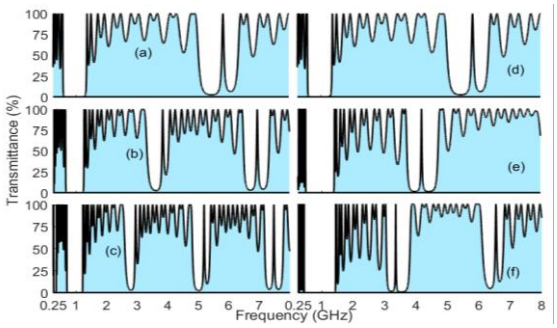

Fig. 4. Transmission spectra with various layer thicknesses. (a)6 mm, (b)12 mm, and (c)18 mm thickness for each DNG material layer. (d)6 mm, (e)12 mm, and (f)18 mm thickness for each ENG material layer

By alternately selecting various layer thicknesses for DNG and ENG material layers, the achieved transmission spectra are illustrated in Fig. 4. Under a determined 6 mm thickness for each ENG (DNG) film condition, Fig. 4(a)-(c) (Fig. 4(d)-(f)) plots the output spectra by selecting the thickness of DNG (ENG) material layer at 6 mm, 12 mm, and 18 mm, respectively, and the repetition rate, 2*N*, of unit cell is fixed at 16, i.e., *N*=8, for total PC. By solely changing the thickness of DNG layer, it can be seen that the widths of two types of band gaps are simultaneously compressed, as shown in Fig. 4(a)-(c). As a result of the increased DNG material layer, the Bragg band gaps and corresponding defect modes are shifted to lower frequencies, and the FWHM of defect modes are also shortened. Here, the Bragg band gap with lowest frequency is called as the first Bragg band gap whose central frequency is low compared to other Bragg band gaps observed in Fig. 4. In contrast, the central position of special band gap is still fixed at about 1 GHz frequency for any DNG layer thickness. Nevertheless, in the case of a determined 6 mm thickness for DNG material layer, the width of special band gap displayed in Fig. 4(d)-(f) is remarkably broadened by enlarging the thickness of ENG material layer to 6 mm, 12 mm, and 18 mm, respectively. In these illustrations, the evolution trends of Bragg band gap and its defect mode are similar to those of Fig. 4(a)-(c), and the central frequency in the special band gap is still insensitive to the change of thickness of ENG layer. Hence, one can conclude that, by synchronously increasing (reducing) the DNG thickness and reducing (increasing) the ENG thickness, i.e., enlarging (decreasing) the thickness ratio of DNG to ENG layers, a narrow (broad) special band gap can be achieved.

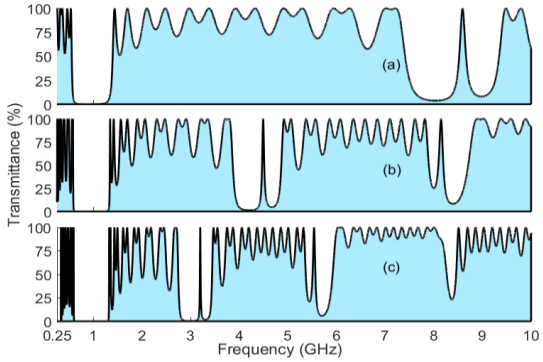

Fig. 5. Transmission spectra for various lattice constants, (a) 8 mm, (b) 16 mm, and (c) 24 mm under thickness ratio of 1 condition

Under a determined thickness ratio of DNG to ENG layers condition, the output spectra that are shown in Fig. 5(a)-(c) are plotted for 8 mm, 16 mm, and 24 mm lattice constants. The thickness ratio of layer *A* to *B* is fixed at 1, and other parameters are identical to those in Fig. 4. In this case, it is seen that the central frequency and width of special band gap nearly aren't changed with the increase of lattice constant that results in the red-shifted Bragg band gap and defect mode. Additionally, widths of Bragg band gap and defect mode are remarkably shortened by enlarging the lattice constant in the case of a determined thickness ratio. Obviously, the exhibited behaviors are similar to those of Fig. 4. Here, it should be noted that, under any fixed thickness ratio condition, the features of special band gap are insensitive to the change of lattice constant. In reality, the red-shifted Bragg band gap and defect mode are attributed to the increase of resonance wavelength, resulting from the extended layer thickness. Because of the combined effects of physical mechanisms in DNG and ENG materials, the special band gap takes on prominent phenomena by means of scale change.

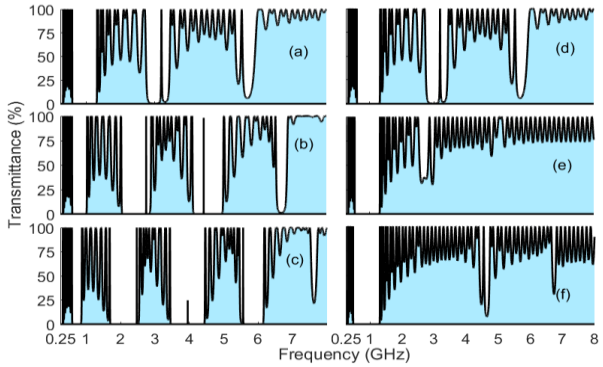

Fig. 6. Transmission spectra with various permittivity and permeability parameters for DNG material. (a)ε_{D0}=2, (b) ε_{D0}=4, (c) ε_{D0}=6, (d)μ_{D0}=4, (e) μ_{D0}=6, and (f) μ_{D0}=8

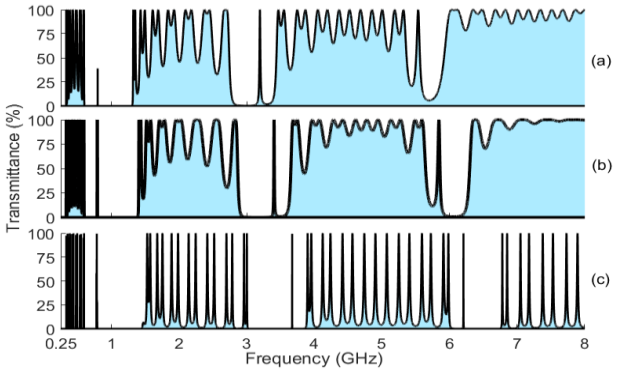

Fig. 7. Transmission spectra with incident angle θ (a) 2^0, (b) 45^0, (c) 85^0, respectively

While parameters of ENG material are selected as ε_{E0}=1, and μ_{E0}=3, the changed spectra are displayed in the cases of various epsilon- and mu-parameters for DNG material, as can be seen in Fig. 6(a)-(c) with ε_{D0}=2, 4, 6, and μ_{D0}=4, as well as Fig. 6(d)-(f) with μ_{D0}=4, 6, 8, and ε_{D0}=2. As the epsilon value of DNG material is increased from 2 to 6, the width of special band gap is remarkably compressed from ~0.7 GHz to ~0.25 GHz. The Bragg band gap and defect mode are further red-shifted, and the defect mode in the first Bragg band gap is also shifted into the adjacent transmission band because of the enhanced refractive index induced by the increased permittivity value. Additionally, it is seen that the transmittances of some defect modes are decreased, and their width becomes narrower in the case of large permittivity parameter. On the other hand, the width of special band gap is slightly broadened from 0.71 GHz to 0.83 GHz as the permeability of DNG material is orderly switched to 4, 6, 8. In this case, some Bragg band gaps are compressed or disappeared as a result of the increase of permeability of DNG material. Therefore, one can see that the permittivity and permeability dependent photonic band gaps take on some different characteristics in comparison to the above output spectra, and it should be pointed out that large permeability value cannot be adopted in order to achieve better Bragg band gap. The materials parameters including permittivity and permeability have strong influences on the special band gap that is insensitive to the scale change for a determined thickness ratio of two layers. Of course, it can be concluded that, by changing the material parameters (ε and μ) of ENG media, the similar results can be obtained compared to the cases of Fig. 6.

When the angles of incidence are taken as $\theta=2^0$, 45^0, and 85^0, respectively, the outcome transmission spectra of the TE polarization wave are displayed in Fig. 7(a)-(c) with 16 pairs of unit cells for the total PC and 6 mm thickness for each dielectric layer. In the case of larger angle of incidence (e.g. 85^0), widths and central positions of Bragg band gaps and special band gap are slightly extended and shifted to higher frequencies, respectively, compared to those of lower incident angle (e.g. 2^0). However, it is shown that, as the incident angle is increased, the band edge located at the side of high frequency for the special band gap is gradually shifted to higher frequency, and its opposite band edge has no any change. In this plot, one can surprisingly find that a resonance mode in the special band gap is exhibited in the case of oblique incidence, in which the output power of resonance mode is also enhanced till to approach 100% as a result of the increase of incident angle. By means of calculations, it is shown that the permeability parameter of DNG material is close to zero as the frequency of incident wave is located at the central frequency of resonance mode for the case of less than 10^0 incident angle. This implies that the special resonance mode is coming from the optical properties of DNG material, and it will be shifted into the adjacent transmission bands by increasing or decreasing the value of permeability of DNG material. Here, in order to clearly observe the influences of incident angle on the defect mode in the first Bragg band gap and the referred resonance mode, their evolutions of angle dependent output spectra are displayed in Figs. (8), and (9) with respect to the incident angle, ranging from 0^0 to 85^0. According to above illustrations, the resonance mode is absent at normal incidence, as can be seen in Fig. 8, in which it is shown that the width of resonance mode is very narrow for less than 10^0 incident angle. The resonance mode is gradually shifted to lower frequency, and further evolved into multi-peaks structure due to the increase of incident angle that also induce the extension of width of resonance mode. Contrarily, the position of defect mode is remarkably shifted to higher frequency against the incident angle, as shown in Fig. 9, where the line-width of defect mode is quickly shortened by increasing the incident angle

and its transmittance is nearly kept at a constant of 100%. Compared to the case of resonance mode, the presented defect mode always maintains the single-peak structure at any incident angle.

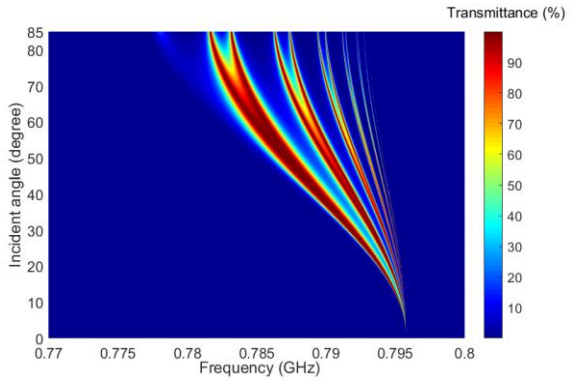

Fig. 8. Spectral evolution of resonance mode in the special band gap as a function of incident angle

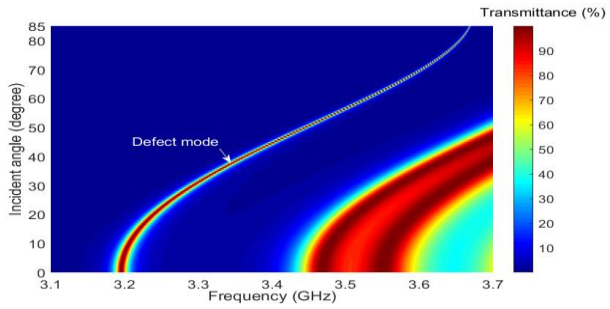

Fig. 9. Spectral evolution of defect mode in the first Bragg band gap as a function of incident angle

4. Conclusion

In conclusion, we present the one-dimensional photonic crystal with $(AB)^N(BA)^N$ structure, in which both layer *A* and layer *B* are made of double-negative and eplison-negative metamaterials, respectively. The optical properties such as photonic band gap, resonance mode, and defect mode of transmission spectra are shown and analyzed as a function of parameters including periodic number, incident angle, permittivity, permeability, layer thickness, as well as lattice constant. Owing to the inherent properties of metamaterials, a special band gap that has lower frequency is achieved in the transmission spectrum, and a resonance mode located within the special band gap is exhibited in the case of oblique incidence. In addition, Bragg band gaps and defect mode are, respectively, observed because of the strong interference of Bragg scattering caused by interface between two layers with different optical properties, and the localized defect layer, i.e., the linking position between $(AB)^N$ and $(BA)^N$. Under the condition of a determined thickness ratio of layer *A* to layer *B*, the width and central frequency of special band gap is insensitive to the lattice constant whose enhancement results in the compression and the red-shifted Bragg band gap and defect mode. For other cases, the influences of various parameters on the transmission spectrum are very strong. Through this study, the metamaterials based one-dimensional photonic crystals will have some potential applications such as tunable filter, optical switching, omnidirectional reflector, and so on.

Acknowledgements

This work was supported in part by the Open Foundation of State Key Laboratory on Integrated Optoelectronics under Grant IOSKL2016KF02.

References

[1] J. D. Joannopoulos, et al., Photonic Crystals Molding the Flow of Light, Princeton University Press, 41 Willian Street, Princeton, New Jersey.
[2] F. C. Peng, M. Y. Jiang, J. W. Wu, Optoelectron. Adv. Mat. **11**(1-2), 12 (2017).
[3] A. Gharaati, N. Miri, Optoelectron. Adv. Mat. **11**(11-12), 608 (2017).
[4] J. Zhang, X. H. Zhao, Y. L. Zheng, H. G. Li, X. F. Chen, Opt. Express **26**(12), 15675 (2018).
[5] A. M. Vyunishev, P. S. Pankin, S. E. Svyakhovskiy, I. V. Timofeev, S. Y. Vetrov, Opt. Lett. **42**(18), 3602 (2017).
[6] C. Li, X. Y. Hu, H. Yang, Q. H. Gong, AIP Adv. **7**(2), 025203 (2017).
[7] Y. Iqbal, M. Faryad, Photon. Nanostruct. **24**, 63 (2017).
[8] S. H. Ryu, M. J. Gim, W. Lee, S. W. Choi, D. K. Yoon, ACS Appl. Mater. Inter. **9**(3), 3186 (2017).
[9] K. X. Dong, D. J. Chen, B. B. Jin, X. S. Jiang, J. P. Shi, IEEE Photonics J. **8**(4), 6804307 (2016).
[10] L. H. Han, L. M. Liu, Z. Y. Yu, H. J. Zhao, X. Song, J. H. Mu, X. Wu, J. J. Long, X. Liu, Chin. Opt. Lett. **12**(1), 010603 (2014).
[11] S. T. M. Fryslie, Z. H. Gao, H. Dave, B. J. Thompson, K. Lakomy, S. Y. Lin, P. J. Decker, D. K. Mcelfresh, J. E. Schutt-Ainé, K. D. Choquette, IEEE Journal of Selected Topics in Quantum Electronics **23**(6), 1700409 (2017).
[12] S. Q. Yan, X. L. Zhu, L. H. Frandsen, S. S. Xiao, N. A. Mortensen, J. J. Dong, Y. H. Ding, Nat. Commun. **8**, 14411 (2017).
[13] Y. Liu, L. Yi, X. G. Hu, Y. F. Duan, Z. Z. Yang, Phys. Plasmas **22**, 012101 (2015).
[14] M. S. Hwang, H. R. Kim, K. H. Kim, K. Y. Jeong, J. S. Park, J. H. Choi, J. H. Kang, J. M. Lee, W. I. Park, J. H. Song, M. K. Seo, H. G. Park, Nano. Lett. **17**(3), 1892 (2017).
[15] S. Surdo, G. Barillaro, Opt. Express **23**(7), 9192 (2015).

[16] H. F. Zhang, S. B. Liu, IEEE Journal of Selected Topics in Quantum Electronics **21**(2), 4900108 (2015).
[17] K. Vaskevicius, M. Gabalis, D. Urbonas, A. Balcytis, R. Petruskevicius, S. Juodkazis, J. Opt. Soc. Am. B **34**(4), 750 (2017).
[18] H. Park, A. Camper, K. Kafka, B. Ma, Y. H. Lai, C. Blaga, P. Agostini, L. F. Dimauro, E. Chowdhury, Opt. Lett. **42**(19), 4020 (2017).
[19] Y. Y. Zhao, S. G. Li, X. Y. Wang, G. Y. Wang, M. Shi, J. J. Wu, Opt. Commun. **400**, 79 (2017).
[20] R. Y. Tang, J. W. Wu, B. Nakarmi, Quantum Electron. **46**(7), 640 (2016).
[21] A. Mendoza-Suarez, H. Perez-Aguilar, Photon. Nanostruct. **14**, 93 (2015).
[22] S. K. Srivastava, A. Aghajamali, Physica B **489**, 67 (2016).
[23] M. Z. Ali, Chin. Opt. Lett. **11**(4), 040501 (2013).
[24] C. J. Wu, M. H. Lee, J. Z. Jian, Progress in Electromagnetics Research-PIER, **136**, 561 (2013).
[25] V. G. Veselago, Sov. Phys. Usp. **10**(4), 509 (1968).
[26] L. J. Dong, G. Q. Du, H. T. Jiang, H. Chen, Y. L. Shi, J. Opt. Soc. Am. B **26**(5), 1091 (2009).
[27] J. A. Monsoriu, R. A. Depine, M. L. Martinez-Ricci, E. Silvestre, Opt. Express **14**(26), 12958 (2006).
[28] J. S. Li, L. Zhou, C. T. Chan, P. Sheng, Phy. Rev. Lett. **90**(8), 083901 (2003).
[29] Y. H. Chen, Opt. Express **18**(19), 19920 (2010).
[30] X. Li, K. Xie, H. M. Jiang, Chin. Opt. Lett. **6**(2), 130 (2008).
[31] H. T. Jiang, H. Chen, H. Q. Li, Y. W. Zhang, Appl. Phys. Lett. **83**(26), 5386 (2003).

*Corresponding author: jwwu@cqnu.edu.cn